East European Journal of Physics. **2.** 280-291 (2026)
DOI:10.26565/2312-4334-2026-2-30 ISSN 2312-4334

STRUCTURAL, OPTOELECTRONIC AND MECHANICAL PROPERTIES OF $AHgCl_3$ (A=Rb, Cs) PEROVSKITES: A FIRST-PRINCIPLES GGA AND TB-mBJ ANALYSIS

Habiba Bouheraoua, El-Djemai Belbacha*
Laboratory of Physico-Chemical Studies of Materials (LEPCM), Department of Physics, Faculty of Matter Sciences, University of Batna 1, 05000 Batna, Algeria
**Corresponding Author e-mail: eldjemai.belbacha@univ-batna.dz*
Received January 27, 2026; revised April 14, 2026; accepted April 25, 2026

The structural, mechanical, and optoelectronic properties of cubic halide perovskites $AHgCl_3$ (A = Rb, Cs) were investigated using density functional theory (DFT) within the full-potential linearized augmented plane wave (FP-LAPW) method, as implemented in the WIEN2k code. The structural stability of the cubic phase was confirmed using the Goldschmidt tolerance factor and the octahedral factor, while the negative formation energies verified their thermodynamic stability. The calculated elastic parameters, including Poisson's ratio, Pugh's ratio, and Cauchy pressure, indicate that both compounds are mechanically stable, ductile, and exhibit a predominantly ionic bonding nature. The optoelectronic properties were examined using the Tran–Blaha modified Becke–Johnson (TB-mBJ) potential. The results reveal that $RbHgCl_3$ and $CsHgCl_3$ are indirect-band-gap semiconductors with band gaps of 1.25 eV and 1.16 eV, respectively. Furthermore, the optical properties were analyzed over the photon energy range of 0–20 eV. Both compounds exhibit strong absorption in the ultraviolet region and low reflectivity at zero photon energy, indicating favorable performance for optoelectronic applications. Overall, these findings suggest that $AHgCl_3$ (A = Rb, Cs) halide perovskites are promising candidates for applications in photovoltaic devices and ultraviolet photodetectors.
Keywords: *Halide perovskite $KZnX_3$; FP-LAPW; Ab-initio; Wien2k; Opto-electronic properties; TB-mBJ*
PACS: 71, 20.Gj, 81.30.-t

1. INTRODUCTION

The exceptional optoelectronic, magnetic ordering, giant magnetoresistance, and thermoelectric properties of perovskites make them intriguing candidates for diverse applications, such as sensors, microelectronics, solar cells, light-emitting diodes, spintronic devices, photovoltaics, and telecommunications devices [1]. In 1839, Gustav Rose discovered the first perovskite, $CaTiO_3$, and the renowned scientist Count Lev Alexeevich von Perovski, after whom the material was named [2]. Consequently, any material exhibiting a comparable structure and employing the chemical formula ABX_3 is designated as a perovskite. This material family comprises conductors, insulators, semiconductors, and superconductors [2].

The cubic perovskite structure has the chemical formula ABX_3, where cations A and B represent alkali and alkaline earth metals, respectively, and X is an anion. Perovskites can be classified into three main groups according to the anion type: oxide (ABO_3), nitride (ABN_3), and halide perovskites ABX_3 (X = F, Cl, Br, I) [3]. To maintain charge neutrality, halide perovskites typically accommodate divalent metal cations in the +2-oxidation state, such as Pb^{2+}, Sn^{2+}, and Ge^{2+} [4]. In addition, halide perovskites can be readily processed into polycrystalline thin films, making them well-suited for optoelectronic applications across various substrates [5]. The remarkable optical and charge-transport properties of halide perovskites have made them widely sought-after light-harvesting materials with appropriate band gaps, high optical absorption coefficients, long charge-carrier diffusion lengths, high external quantum efficiency, and a notable defect tolerance [6]. In addition, several halide perovskite crystallographic phases have been identified at different temperatures, and cubic, tetragonal, and orthorhombic are the most prevalent phases [7]. Chloroperovskites$ABCl_3$ have a wide band gap, which qualifies them for use in numerous contemporary energy storage devices. Moreover, the broad band gap energy enables chloroperovskites to effectively emit or absorb ultraviolet radiation, rendering them desirable for optoelectronic devices [8-10].

Some examples of cubic halide perovskites are $CsZnCl_3$ and $KHgCl_3$. These compounds were theoretically studied by Aqili et al. [11] and Ullah et al [12]. Their findings indicated that these cubic halide perovskites are indirect band gap semiconductors with band gaps of 3.628 and 1.11 eV, respectively, and might be viable candidates for UV optoelectronic applications [11-12]. M. Arif et al. [13] examined the physical properties of cesium-based cubic halide perovskites, $CsHgX_3$ (X = F, Cl), employing the full potential linearized augmented plane wave (FP-LAPW) approach under the generalized gradient approximation (GGA). Their findings, which include electronic band structure and density of states calculations, revealed that $CsHgF_3$ has an indirect band gap and behaves as a semiconductor, whereas $CsHgCl_3$ exhibits metallic behavior. In the same vein, we have thoroughly investigated the perovskites $RbHgCl_3$ and $CsHgCl_3$. These compounds are documented as stable in the Open Quantum Materials Database (OQMD) [14-15]. We present theoretical calculations on $AHgCl_3$ (where A = Rb or Cs) halide perovskite compounds, providing us with important information about their structural, elastic, and optoelectronic properties, employing the full potential

Cite as: H. Bouheraoua, El-D. Belbacha, East Eur. J. Phys. 2, 280 (2026), https://doi.org/10.26565/2312-4334-2026-2-30

linearized augmented plane wave (FP-LAPW) method within the generalized gradient approximation (GGA) and the Tran and Blaha modified Becke Johnson (TB-mBJ) approach for optoelectronic characteristics. The following is the structure of the study: Section 1 presents a concise introduction, and Section 2 delineates the computational methodologies employed in this investigation. Further, we present our findings in Section 3. Finally, we summarize our results and provide the conclusions.

2. COMPUTATIONAL DETAIL

The physical properties of halide perovskites with a cubic structure, $AHgCl_3$ (A=Rb, Cs), were calculated using the Wien2k package [16] based on the full potential linearized augmented plane wave (FP-LAPW) method [17] to solve the Kohn–Sham equations [18]. This approach is predicated on density functional theory (DFT) [19]. To determine the most stable ground state of the compounds, we optimized the structures using different exchange correlation potentials, including PBE [20], WC [21], and PBE-sol [22]. The Murnaghan equation of state [23] was employed to determine the equilibrium lattice parameters by fitting the total energy–volume data points. The optoelectronic properties were investigated using the Tran–Blaha modified Becke–Johnson (TB-mBJ) [24] and GGA-PBE [20] potentials. The shifted k-point mesh was set to 14×14×14, which corresponds to a dense mesh of 3000 k-points in the first Brillouin zone. The cutoff of the plane waves, RMT×Kmax = 8, was chosen for the interstitial area, whereas the maximum value for the wave function expansion inside spheres was Lmax = 10. In addition, the Fourier charge density inside the atomic sphere was set to Gmax = 12 (a.u.) $^{-1}$, and the cutoff energy was chosen to be − 6.00 Ryd. The self-consistent cycles converged when the total energy was stable within 10^{-5} Ryd. Moreover, the elastic constants examined in this study were obtained using the IRelast [25] method integrated into the Wien2k software [16].

3. RESULTS AND DISCUSSION

3.1 Structural Properties

The perovskite $AHgCl_3$ (A = Rb, Cs) crystallizes in space group 221 (Pm-3m), with lattice properties detailed in Table 1. The A atom is located at (0, 0, 0), the Hg atom is positioned at the center, and the Cl atoms are placed at the face centers (0.5, 0.5, 0), (0, 0.5, 0.5), and (0.5, 0, 0.5) of the lattice. Figure 1 illustrates the crystal structures of $AHgCl_3$ (A = Rb, Cs) perovskites.

Table 1. Computed lattice parameters (A°), volume V ($a.u^3$), bulk modulus B (GPa), pressure derivative B', minimum energy E_0 (Ryd), formation energy E_{form} (eV/atom) values for $AHgCl_3$ (A= Rb, Cs)

Compound	XC	a	V	B	B'	E_0	E_{form}	t	μ
$RbHgCl_3$	PBE	5.37	1045.14	28.43	5.25	-48056.066643	-0.63	0.832	0.657
	WC	5.26	986.13	33.17	5.33	-48050.776143			
	PBE-sol	5.25	979.85	34.51	5.39	-48037.487811			
Other works	[14-15]	5.32							
$CsHgCl_3$	PBE	5.41	1068.74	27.74	5.31	-57673.688577	-0.57	0.870	0.657
	WC	5.28	998.93	33.63	5.50	-57667.866339			
	PBE-sol	5.28	995.65	34.34	5.16	-57652.563214			
Other works	[14-15]	5.38							
	[13]	5.40							

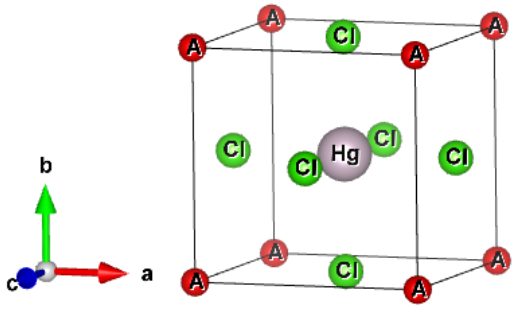

Figure 1. Crystal structure of cubic halide perovskites $AHgCl_3$ (A=Rb, Cs)

Furthermore, to validate the structural stability of these perovskites, we employed the tolerance factor t and the octahedral factor μ. These two quantities are related to the ionic radii using the following equations [26, 27]:

$$t = \frac{R_A + R_X}{\sqrt{2}(R_B + R_X)} \tag{1}$$

$$\mu = \frac{R_B}{R_X} \tag{2}$$

For the cubic perovskite structure, the tolerance factor must lie within the range of $0.8 \leq t \leq 1.0$, and μ is known to be between 0.377 and 0.895 [26, 27]. The values of t and μ are presented in Table 1, which demonstrates that all crystal structures are stable and have cubic symmetry. We computed the formation energy using Equation (3) [28] to discuss the thermodynamic stability.

$$E_f = \frac{1}{5}\left[E_{tot}^{AHgCl_3} - \left(E_a^A + E_a^{Hg} + 3E_a^{Cl} \right) \right], \tag{3}$$

where $E_{tot}^{AHgCl_3}$represent the total energy of the $AHgCl_3$ compound and $E_a^A, E_a^{Hg} and E_a^{Cl}$ are the total energies of A, Hg, and Cl, respectively.

The calculated formation energies of $RbHgCl_3$ and $CsHgCl_3$ are listed in Table 1 and obey the criterion of Ef < 0.2 eV/atom [1], ensuring that these formation materials can be formed experimentally. In addition, negative formation energies indicate thermodynamic stability.

The calculated values of the lattice parameters, volume, bulk pressure, derivative, ground state, and formation energies for the compounds are listed in Table 1. This table shows that the minimum energy for $AHgCl_3$perovskites corresponds to the GGA-PBE, that is, − 48056.066643 Ryd ($RbHgCl_3$) and − 57673.688577 Ryd ($CsHgCl_3$), indicating that RbHgCl3 and $CsHgCl_3$ remain stable in the GGA-PBE. Fig. 2 illustrates the structural optimization curves for $RbHgCl_3$ and $CsHgCl_3$ compounds using a GGA-PBE approximation.

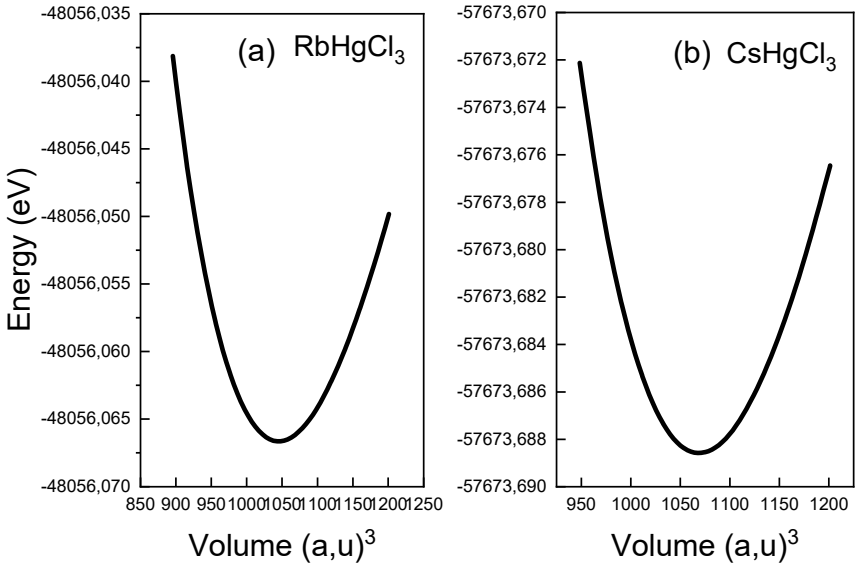

Figure 2. The variation of the total energy as a function of volume for (a) $RbHgCl_3$, (b) $CsHgCl_3$ with GGA-PBE

3.2 ELECTRONIC PROPERTIES

To investigate the electronic properties of cubic halide perovskites $AHgCl_3$ (A = Rb, Cs), we computed the energy band structure (BS), total density of states (TDOS), and partial density of states (PDOS) along high-symmetry directions within the first Brillouin zone over an energy range of −14 to 14 eV using both the GGA-PBE and TB-mBJ approximations. Figures 3(a) and (b) present the band structures of both compounds, with the Fermi level indicated by a horizontal red dashed line at 0 eV.

The GGA-PBE results indicate metallic behaviour in both $RbHgCl_3$ and $CsHgCl_3$, as the valence and conduction bands overlap at the Fermi level, resulting in no band gap. Although these findings are consistent with the values reported in the OQMD database [14,15], this metallic prediction highlights a well-known limitation of GGA, which systematically underestimates band gaps in semiconductors and insulators.

To address this limitation, the TB-mBJ potential was applied, which yielded a more accurate depiction of the electronic structure. The TB-mBJ calculations revealed that both compounds are indirect semiconductors, with the valence band maximum (VBM) at the L point and the conduction band minimum (CBM) at the Γ point (L–Γ). The band gap values listed in Table 2 underscore the substantial improvement provided by the TB-mBJ in accurately capturing the semiconducting nature of these halide perovskites.

The analysis of the total and partial densities of states provides valuable insights into the bonding properties and the nature of the electronic band structure. The total (TDOS) and partial (PDOS) densities of states for $RbHgCl_3$ and $CsHgCl_3$ were calculated using the TB-mBJ potential, as shown in Figs. 3(a, b) and 4(a–f), respectively. The TDOS profiles of all compounds clearly reveal the bandgap (Eg), confirming their semiconducting nature. For $AHgCl_3$ (A = Rb, Cs), the valence band primarily originates from A(p), Hg(d), and Cl(s+p) orbitals, whereas the conduction band is mainly composed of A(d) states, with significant contributions from Hg(d).

Table 2. Calculated indirect band gaps (eV) for $RbHgCl_3$ and $CsHgCl_3$ using GGA-PBE and TB-mBJ

Compound	XC	Bandgap	Other works
$RbHgCl_3$	PBE	0.00	0.00[14-15]
	TB-mBJ	1.25	
$CsHgCl_3$	PBE	0.00	0.00[13-14-15]
	TB-mBJ	1.16	

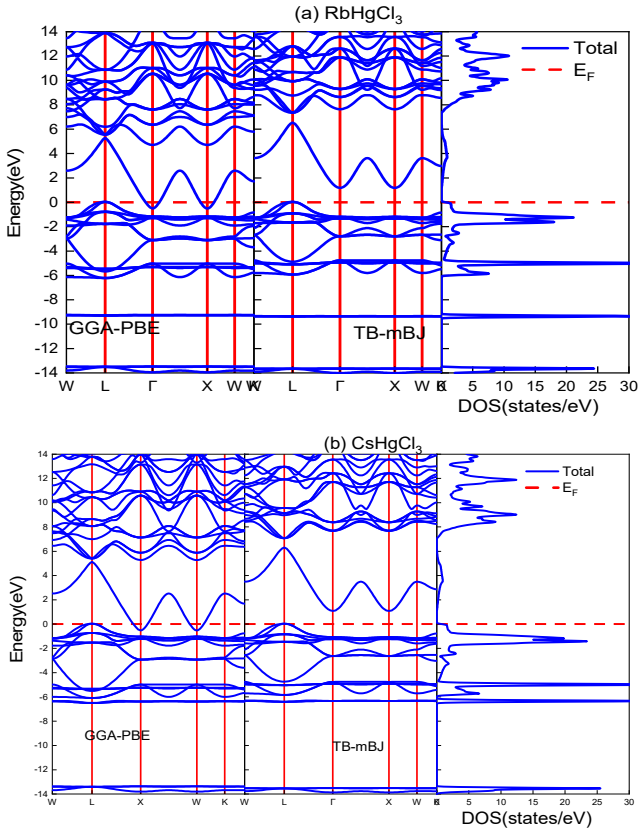

Figure 3. Band structure and DOS for(a) $RbHgCl_3$and (b) $CsHgCl_3$compounds

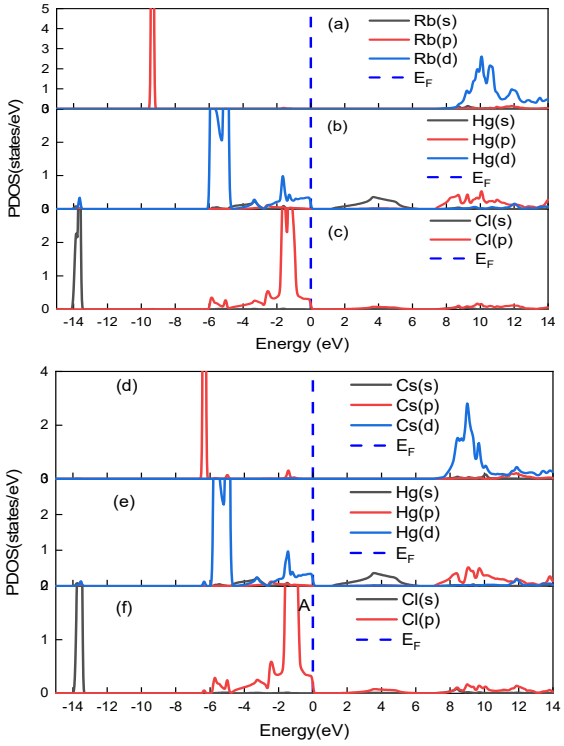

Figure 4. Computed partial densities of states of $AHgCl_3$ compound with TB-mBJ

3. MECHANICAL PROPERTIES

Elastic constants (Cij) are fundamental parameters for describing the mechanical properties of materials. These constants characterize the response of a crystal to external forces. A material is considered mechanically stable if it satisfies the Born stability criteria [29–31]: $C_{11} - C_{12} > 0$, $C_{44} > 0$, $C_{11} > 0$, $(C_{11} + 2C_{12}) > 0$, and $C_{12} < B < C_{11}$. The results presented in Table 3 satisfy these stability criteria, indicating that all the compounds are mechanically stable. Furthermore, the elastic constants can be used to evaluate key mechanical parameters, such as the bulk modulus (B), shear modulus (G), and Young's modulus (E). The relationships between these parameters and the elastic constants are expressed in Eqs. (4)–(8).

$$B = \frac{C_{11} + 2C_{12}}{3} \tag{4}$$

$$G_V = \frac{C_{11} + 3C_{44} - C_{12}}{5} \tag{5}$$

$$G_R = \frac{5(C_{11} - C_{12})C_{44}}{3(C_{11} - C_{12}) + 4C_{44}} \tag{6}$$

$$G = \frac{1}{2}(G_V + G_R) \tag{7}$$

$$E = \frac{9BG}{3B + G} \tag{8}$$

The shear modulus (G) characterizes the stiffness of a material and is defined by Eqs. (5) – (7), where G_V, G_R, and G represent the Voigt [32], Reuss [33], and Hill average shear moduli, respectively. A low value of G indicates that the material is more flexible and easily deformed under shear stress.

The bulk modulus (B) measures the resistance of a material to compression, as expressed in Eq. (4). The relatively low values of B suggest the softness and flexibility of the studied compounds. As shown in Table 3, the bulk modulus (B) values for all compounds are low and of similar magnitude, which further confirms their mechanical softness. Consequently, the shear modulus G is lower than the bulk modulus B, indicating that the analyzed compounds exhibit greater resistance to volumetric compression than to shear deformation.

Young's modulus (E), which depends on both the bulk modulus (B) and shear modulus (G), as given in Eq. (8), provides a measure of the stiffness of the material. The rigidity of a compound increases with increasing Young's modulus. The calculated values of B, G, and E, presented in Table 3, indicate that the ternary chloroperovskite compounds $AHgCl_3$ (A = Rb, Cs) possess moderate rigidity.

To further evaluate the ductile or brittle nature of these compounds, additional mechanical parameters, including Poisson's ratio, Pugh's ratio, and Cauchy pressure, were determined, as listed in Table 3. According to Eq. (9), a material is considered more stable against external deterioration and less compressible when the Poisson's ratio lies between 0.25 and 0.5 [1,34–35].

$$\upsilon = \frac{1}{2}\left[\frac{3B - 2G}{3B + G}\right] \tag{9}$$

Poisson's ratio typically takes values of approximately 0.33 for ionic bonding, 0.25 for metallic bonding, and 0.1 for covalent bonding [1]. Furthermore, Frantsevich et al. [36] reported that a material is classified as ductile if its Poisson's ratio exceeds 0.26 and as brittle if it is below this threshold. The calculated Poisson's ratio values are greater than 0.26, suggesting that the studied compounds exhibit ductile behavior and a predominantly ionic bonding characteristics.

The ratio of the bulk modulus to the shear modulus (B/G), known as Pugh's ratio (K) [37], is another important ductility indicator. A material is considered brittle when (B/G) < 1.75; otherwise, it is considered ductile. In the present study, the calculated Pugh's ratio exceeded 1.75, further confirming the ductile nature of the compounds.

The Cauchy pressure ($CP = C_{12} - C_{44}$) [38] is also used to distinguish between ductile and brittle behaviors. Negative CP values indicate brittleness, whereas positive values suggest ductility. The calculated CP values (Table 3) were positive, indicating that all compounds exhibited ductile behavior.

Another important parameter used to evaluate the presence of microcracks and the mechanical stability of materials is the elastic anisotropy, as determined using Eq. (10).

$$A = \frac{2C_{44}}{(C_{11} - C_{12})} \tag{10}$$

For an isotropic material, A = 1, whereas values of A greater than or less than 1 indicate anisotropic behavior. The calculated values of A, presented in Table 3, show that all compounds exhibit significant anisotropy.

Table 3. Elastic constants C_{11}, C_{12}, and C_{44} (GPa); bulk modulus B (GPa); the shear modulus G (GPa); Young's modulus E (GPa); anisotropic parameter A; Paugh's ratio K; Cauchy pressure C_P; and Poisson's ratio υ for $AHgCl_3$ (A= Rb, Cs) compounds

Compound	C_{11}	C_{12}	C_{44}	B	G	E	A	B/G	C_P	υ
$RbHgCl_3$	46.04	19.71	8.31	28.49	10.00	26.85	0.63	2.84	11.40	0.34
$CsHgCl_3$	45.10	19.41	10.03	27.98	11.07	29.35	0.78	2.52	9.38	0.32
Other works	44.90	18.70	7.56	27.43	9.43	25.40	0.57	2.90	/	0.49

The isotropic and anisotropic characteristics of materials can be elucidated through three-dimensional (3D) representations of the directional dependence of the Young's modulus, shear modulus, and Poisson's ratio. The degree of anisotropy is reflected by the extent to which the resulting closed three-dimensional (3D) surface deviates from an ideal spherical shape. The ELATE tool [39] was used to generate the 3D distributions of Young's modulus (E), shear modulus (G), and Poisson's ratio for $AHgCl_3$ (A = Rb, Cs), as shown in Fig. 5. The studied halide perovskites $AHgCl_3$ (A = Rb, Cs) exhibit anisotropic behavior.

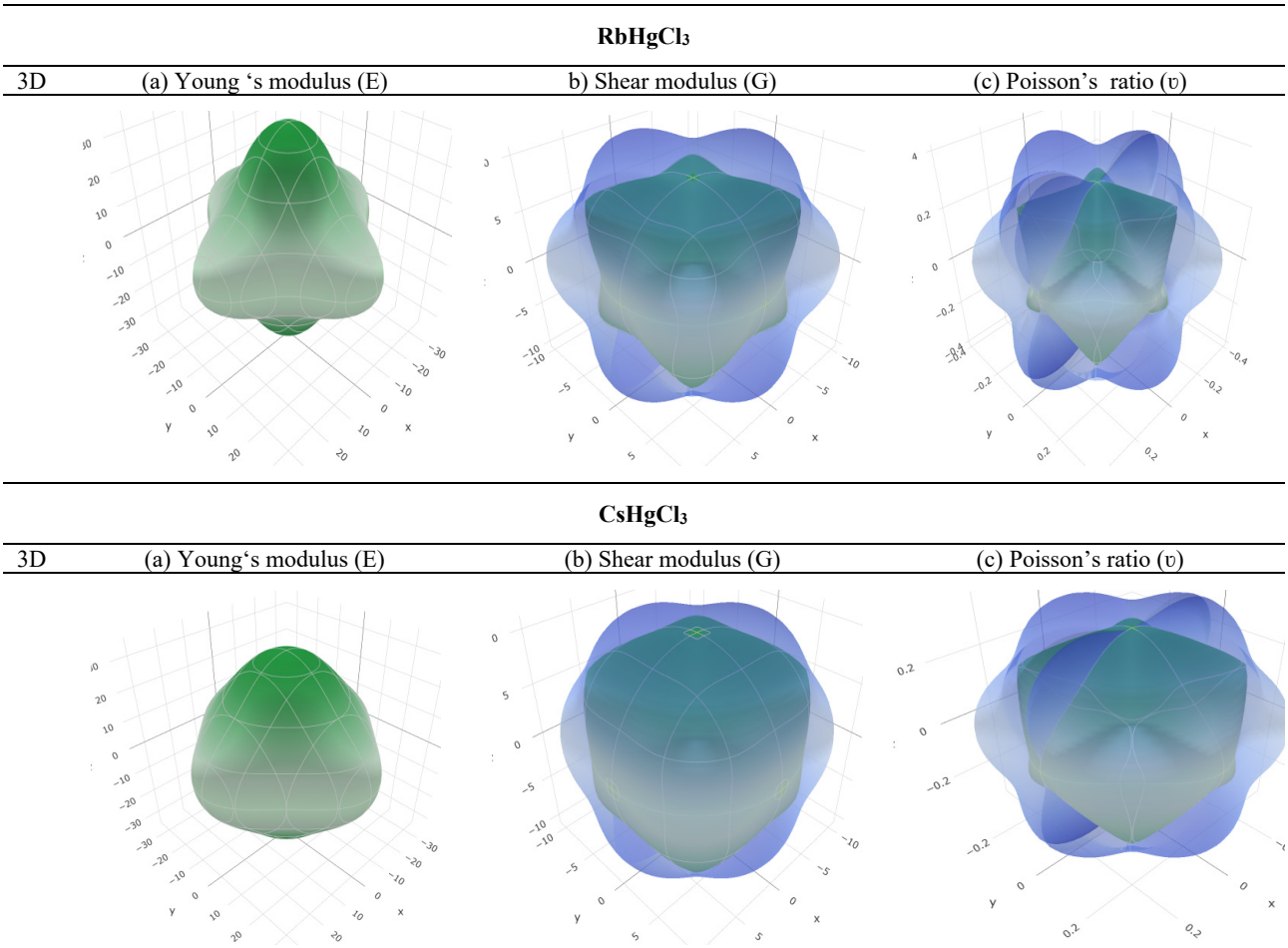

Figure 5. (3D): Young's modulus (a) (E(GPa)), shear modulus (b) (G(GPa)), and Poisson's ratio υ (d) for $AHgCl_3$ (A= Rb, Cs) compounds

3. 4 THERMAL PROPERTIES

Comprehending the velocity of sound, melting point, and Debye temperature is crucial for numerous applications. The computed values of these parameters are presented in Table 4.

Table 4. The calculated values of longitudinal velocity v_l(m/s), transverse velocity v_t,(m/s), sound velocityv_m(m/s), melting temperature T_m,(°K), and Debye temperature θ_D(°K)

Compound	v_l	v_t	v_m	T_m	θ_D
$RbHgCl_3$	3135.04	1541.77	1731.78	825.13	164.16
$CsHgCl_3$	3044.35	1549.69	1736.58	819.58	163.41

The longitudinal and transverse elastic wave velocities [40] were used to estimate the sound velocity [41] using the following equations:

$$\begin{cases} v_l = \sqrt{\dfrac{G}{\rho}} \\ v_l = \sqrt{\dfrac{3B+4G}{3\rho}} \\ v_m = \left[\dfrac{1}{3}\left(\dfrac{2}{v_l^3}+\dfrac{1}{v_l^3}\right)\right]^{-\frac{1}{3}} \end{cases} \tag{11}$$

Where ρ is the mass density of the material, and G and B are the shear and bulk modulus. The data presented in Table 4 indicate that the sound velocity in $RbHgCl_3$ is higher than that in $CsHgCl_3$, which can be attributed to the lower atomic mass of Rb relative to that of Cs.

The thermodynamic properties of a material, including the longitudinal and transverse sound velocities, specific heat, and thermal expansion coefficient, can be correlated with the Debye temperature. The Debye temperature is calculated using the following expression [41]:

$$\theta_D = v_m \frac{h}{K_B}\left[\frac{3n\rho N_A}{4\pi M}\right]^{\frac{1}{3}} \tag{12}$$

Where N_A is Avogadro's number, K_B is Boltzmann's constant, h is Planck's constant, and ρ is the density of thesolid's molecular mass.

The lower sound velocity in $RbHgCl_3$ and $CsHgCl_3$ leads to a corresponding decrease in the Debye temperature. Another important property that can be estimated from the elastic constants is the melting temperature, which can be calculated using the relationship proposed by Fine et al. [42].

$$T_m = \left[553(K) + \left(5.911\left(\frac{K}{GPa}\right)\right)C_{11}\right] \pm 300K \tag{13}$$

3.5 OPTICAL PROPERTIES

Understanding optical parameters, such as the absorption coefficient, refractive index, reflectivity, energy-loss function, extinction coefficient, and optical conductivity, is essential for characterizing interactions between materials and electromagnetic radiation.

The optical properties of the $AHgCl_3$ (A = Rb, Cs) halide perovskites were calculated using the TB-mBJ potential. The analysis begins with a fundamental optical quantity, namely, the complex dielectric function, which is expressed as follows:

$$\varepsilon(\omega) = \varepsilon_1(\omega) + i\varepsilon_2(\omega) \tag{14}$$

For incident photon energies ranging from 0 to 20 eV, the dielectric function ε(ω) was employed to determine the fundamental optical properties using the following relations:

$$\alpha(\omega) = \left[\sqrt{\varepsilon_1^2(\omega)+\varepsilon_2^2(\omega)} - \varepsilon_1(\omega)\right]^{\frac{1}{2}} \tag{15}$$

$$n(\omega) = \frac{1}{\sqrt{2}}\left[\sqrt{\varepsilon_1^2(\omega)+\varepsilon_2^2(\omega)} + \varepsilon_1(\omega)\right]^{\frac{1}{2}} \tag{16}$$

$$R(\omega) = \frac{(1-n)^2 + k}{(1+n)^2 + k} \tag{17}$$

$$L(\omega) = \frac{\varepsilon_1(\omega)}{\varepsilon_1^2(\omega)+\varepsilon_2^2(\omega)} \tag{18}$$

$$K(\omega) = \frac{(\sqrt{2}\omega)}{c}\left[\sqrt{\varepsilon_1^2(\omega)+\varepsilon_2^2(\omega)} - \varepsilon_1(\omega)\right]^{\frac{1}{2}} \tag{19}$$

$$\sigma(\omega) = \frac{\omega\varepsilon_2(\omega)}{4\pi} \tag{20}$$

Fig. 6 presents our results concerning the real part of the dielectric function, the imaginary part of the dielectric function, the absorption coefficient, the refractive index, the reflectivity, the energy loss, the extinction coefficient, and the optical conductivity.

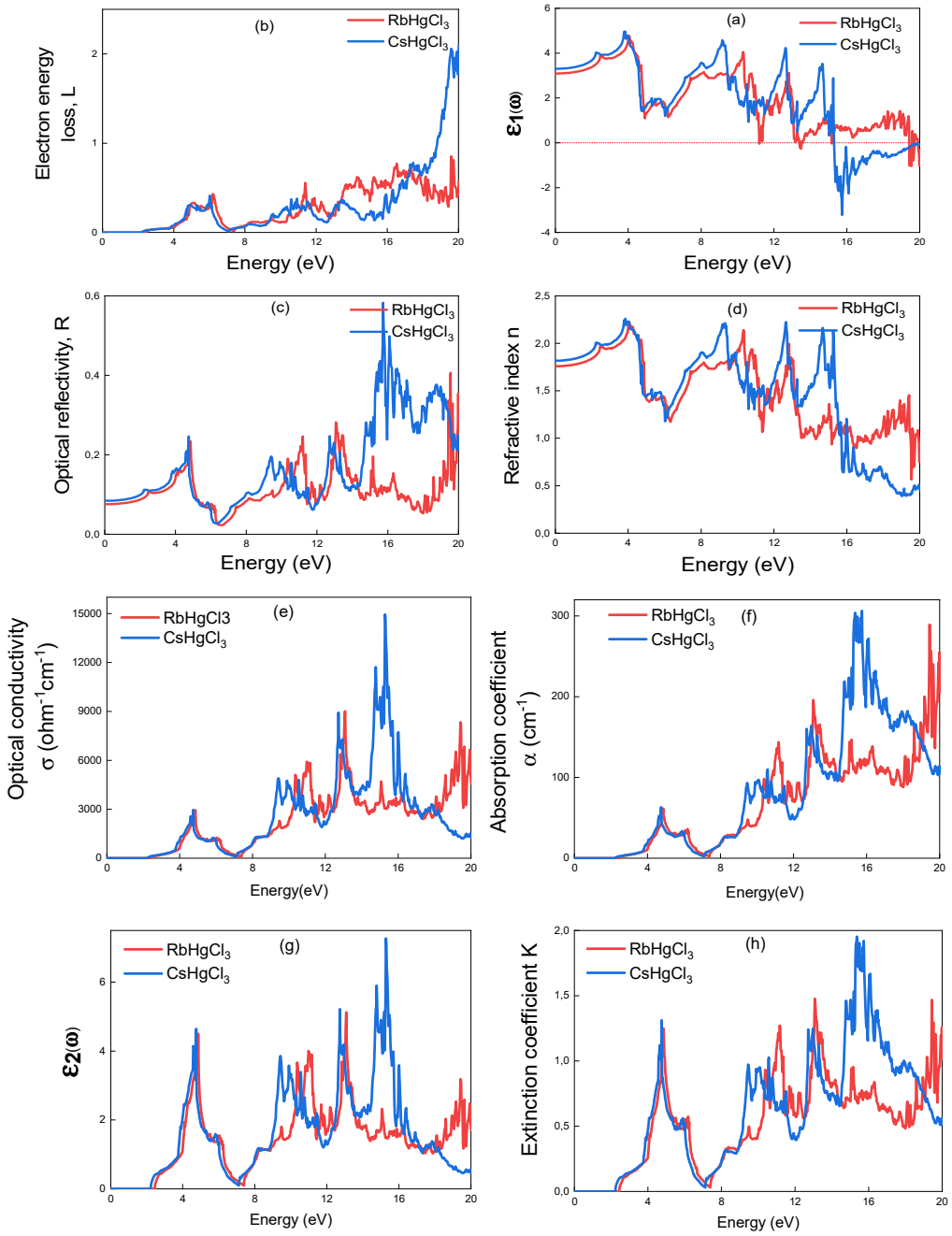

Figure 6. The curve of (a) the imaginary part ε2(ω) of the dielectric, (b) optical conductivity σ(ω), (c) absorption coefficient α(ω), (d) extinction coefficient K(ω), (e) the real part ε1(ω) of the dielectric, (f) refractive index n(ω), (g) optical reflectivity R(ω), and (h) loss function L(ω) of AHgCl3 (A=Rb, Cs).

3.5.1 The real $\varepsilon_1(\omega)$ and imaginary $\varepsilon_2(\omega)$ part of the dielectric function.

The real part of the dielectric function (Fig. 6a) describes the dispersion behavior of the material as well as its polarization capability. The calculated values for $AHgCl_3$ (A = Rb, Cs) halide perovskites are summarized in Table 5, indicating that $RbHgCl_3$ and $CsHgCl_3$ exhibit nearly identical polarization values.

Table 5. Computed the static dielectric function ε_1 (0), static refractive index n (0), and reflective index R(0) for $RbHgCl_3$ and $CsHgCl_3$ utilizing the TB-mBJ approximation

Compound	$\varepsilon_1(0)$	$\varepsilon_1(0)$	*R(0)*
$RbHgCl_3$	3.09	1.75	0.075
$CsHgCl_3$	3.30	1.81	0.084

This behavior can be attributed to the inverse relationship between the band gap and the dielectric response, as described by Penn's model [43], wherein a smaller band gap corresponds to a higher dielectric constant. For both $RbHgCl_3$ and $CsHgCl_3$, the values remain nearly constant throughout the visible region (1.58–3.26 eV). Beyond this range, they increase and reach their maximum values in the ultraviolet region. As illustrated in Fig. 6a, the peak values are 4.78 and 4.96 at photon energies of 4.01 eV and 3.82 eV for $RbHgCl_3$ and $CsHgCl_3$, respectively.

Moreover, within specific energy ranges, the real part becomes negative for both compounds, indicating metallic behavior in these regions.

The imaginary part of the dielectric function is closely related to the electronic band structure and accounts for the absorptive behavior of the material. As shown in Fig. 6g, the imaginary dielectric function of $AHgCl_3$ (A = Rb, Cs) exhibits multiple peaks corresponding to electronic transitions from the valence band to the conduction band. The critical (threshold) energies are determined to be 2.46 eV and 2.24 eV for $RbHgCl_3$ and $CsHgCl_3$, respectively.

The maximum peak values reach 5.12 at 13.07 eV for $RbHgCl_3$ and 7.27 at 15.27 eV for $CsHgCl_3$. These results indicate that absorption begins at approximately 2.46 eV and 2.24 eV for $RbHgCl_3$ and $CsHgCl_3$, respectively, with the strongest absorption occurring in the ultraviolet region.

3.5.2 The absorption coefficient$\alpha(\omega)$

The absorption coefficient, which quantifies the attenuation of light intensity per unit length within a material, exhibits behavior similar to that of the imaginary part of the dielectric function, $\varepsilon_2(\omega)$, as illustrated in Fig. 6f.

For $RbHgCl_3$ and $CsHgCl_3$, absorption begins at 2.46 eV and 2.24 eV, respectively, with maximum values of 289.93 cm^{-1} at 19.44 eV and 306.28 cm^{-1} at 15.74 eV.

These results suggest that both compounds are promising candidates for optoelectronic applications in the ultraviolet region.

3.5.3Optical conductivity $\sigma(\omega)$

The electrical conductivity of the material is described in terms of its optical conductivity, which characterizes its response to electromagnetic radiation. Figure 6(e) shows the optical conductivity $\sigma(\omega)$, which begins at 2.46 eV for $RbHgCl_3$ and 2.24 eV for $CsHgCl_3$.This behavior reflects the strong correlation between $\sigma(\omega)$, the absorption coefficient $\alpha(\omega)$, and the imaginary part of the dielectric function $\varepsilon_2(\omega)$. The maximum optical conductivity reaches 9012.45 $\Omega^{-1}\cdot cm^{-1}$ at 13.07 eV for $RbHgCl_3$, while for $CsHgCl_3$ it reaches 9893.50 $\Omega^{-1}\cdot cm^{-1}$ at 15.74 eV.

These results indicate that the ternary $AHgCl_3$ (A = Rb, Cs) perovskite compounds are promising candidates for ultraviolet optoelectronic device applications.

3.5.4 The extinction coefficient K$(\omega)$and refraction indexn(ω)

The propagation of electromagnetic radiation through a material can be described using the complex refractive index [44]:

$$N(\omega) = n(\omega) + iK(\omega) \tag{21}$$

where $K(\omega)$denotes the extinction coefficient and $n(\omega)$represents the refractive index. The extinction coefficient quantifies the attenuation of light intensity in a material owing to absorption and scattering effects.

As illustrated in Fig. 6h, the spectrum of $K(\omega)$for both compounds closely follows that of the imaginary part of the dielectric function, $\varepsilon_2(\omega)$, owing to their strong correlation, as expressed by the relation$2n(\omega)K(\omega) = \varepsilon_2(\omega)$ [6] .The $K(\omega)$spectra exhibit several pronounced peaks in the ultraviolet region, indicating enhanced optical absorption in this energy range.

The refractive index $n(\omega)$describes the phase velocity of light within the material. Furthermore, as shown in Fig. 6d, the behavior of $n(\omega)$is consistent with that of the real part of the dielectric function, $\varepsilon_1(\omega$, presented in Fig. 6a. The static values of $n(\omega)$and $\varepsilon_1(\omega)$listed in Table 5 further support this relationship [45–46].

$$n_0(\omega) = \sqrt{\varepsilon_1}(\omega) \tag{22}$$

3.5.5 The energy loss function L(ω)

Figure 6(b) depicts the energy-loss function, which describes the energy dissipation of fast electrons in the material owing to electromagnetic radiation and provides insight into the plasmonic response of the system.

The energy-loss spectrum indicates that the dominant losses occur in the ultraviolet region, wherein $RbHgCl_3$ and $CsHgCl_3$ exhibit their maximum peak values. Negligible losses are observed in the visible region and at lower photon energies, indicating reduced plasmonic excitations in these energy ranges.

3.5.6 The optical reflectivity R(ω)

Figure 6(c) illustrates the optical reflectivity, $R(\omega)$, indicating that most of the reflectivity peaks occur in the ultraviolet region at higher photon energies. This behavior corresponds to energy regions where the real part of the dielectric function, $\varepsilon_1(\omega)$, decreases and becomes negative.

The static reflectivity values R(0)for $RbHgCl_3$ and $CsHgCl_3$ are listed in Table 5. The maximum reflectivity values are 0.50 and 0.58 for $RbHgCl_3$ and $CsHgCl_3$, respectively. A low R(0) value for both compounds indicates weak reflectivity and strong absorption in the low-photon-energy region, which is characteristic of semiconductor materials.

This optical behavior suggests that both halide perovskite compounds exhibit similar properties and are promising candidates for optoelectronic applications, particularly in photovoltaic devices and ultraviolet photodetectors.

4. CONCLUSIONS

In this work, the structural, electronic, mechanical, and optical properties of cubic halide perovskites $AHgCl_3$ (A = Rb, Cs) were systematically investigated using density functional theory (DFT) within the FP-LAPW method as implemented in the WIEN2k package.

The structural stability of the cubic phase was confirmed through tolerance and octahedral factor analyses, while the negative formation energies further verified their thermodynamic stability. The mechanical properties indicate that both compounds are mechanically stable, ductile, anisotropic, and predominantly ionic in nature.

Electronic structure calculations using the TB-mBJ potential reveal that $RbHgCl_3$ and $CsHgCl_3$ are indirect band gap semiconductors, with band gap values of 1.25 eV and 1.16 eV, respectively.

The optical analysis demonstrates strong absorption in the ultraviolet region, low reflectivity at zero photon energy, and consistent behavior across key optical parameters, indicating favorable optoelectronic performance.

Overall, the obtained results suggest that both $AHgCl_3$ (A = Rb, Cs) halide perovskites are promising candidates for optoelectronic applications, particularly in photovoltaic devices and ultraviolet photodetectors.

Data Availability

The corresponding author, El-Djemai Belbacha, is available to provide the data supporting this study's findings upon reasonable request.

Conflicts of Interest

The authors of this work (Habiba Bouheraoua and El-Djemai Belbacha) declare that they have no conflicts of interest.

ORCID

Habiba Bouheraoua, https://orcid.org/0009-0008-1254-1943;**Belbacha El-Djemai,** https://orcid.org/0000-0002-2875-1266

REFERENCES

[1] P. Kumari, R. Sharma, U. Lilhore, R. Khenata, and V. Srivastva, "First-principles study on structural, electronic, elastic, mechanical, thermodynamic, and thermoelectric properties of $RbSnX_3$(X= F, Cl, and Br) perovskites," J. Energy Research, **46**, 23893 (2022). https://doi.org/10.1002/er.8687

[2] S. Gupta, S. Singh, R.R. Chaudhary, D. Shikha, and V. Singh, "Review: perovskite materials, properties, and their multifunctional applications," J. Mech. Eng. **7**, 44 (2022).

[3] S.C. Mouna, M. Radjai, A. Bouhemadou, D. Houatis, D. Allali, S.S. Essaoud, and S. Bin-omran, "Structural, elastic, and thermodynamic properties of $BaXCl_3$(X=Li, Na) perovskites under pressure effectab-initio exploration," Physica Scripta, **98**, 065949 (2023).https://doi.org/10.1088/1402-4896/acd3c4

[4] S. Seok, and T.F. Guo, "Halide perovskite materials and devices," MRS Bulletin, **45**, 427 (2020). https://doi.org/10.1557/mrs.2020.140

[5] F. Erdinc, E.K. Dogan, and H. Akkus, "Investigation of structural, electronic, optic, and elastic properties of perovskite $ReGeCl_3$ crystal: a first principles study," Gaz University Journal of science, **32**, 1008 (2019). https://doi.org/10.35378/gujs.448378

[6] S. Naseem, N.A. Noor, R. Ashraf, F. Alresheedi, M. Laraib, A. Rehman, and S. Raiz, "DFT based study of copper calcium halide perovskite nanomaterials for optoelectronic and energy applications," Results in Physics, **58**, 107485 (2024). https://doi.org/10.1016/j.rinp.2024.107485

[7] S. Bouchikhi, K. Benyahia, R. Mehyaoui, and A. Touia, "First principles calculations of the inorganic halide perovskite $RbSnBr_3$: optical and thermoelectric properties of its three phases," Computational Condensed Matter, **33**, e00761 (2022). https://doi.org/10.1016/j.cocom.2022.e00761

[8] M. Husain, N. Rahman, M. Albalawi, S. Ezzine, M. Amami, T. Zaman, A. Rehman, *et al*., "Examining computationally the structural, elastic, optical and electronic properties of $CaQCl_3$(Q=Li and K) Chloroperovskites using DFT framework," RSC advances, **12**, 32338 (2022). https://doi.org/10.1039/d2ra05602j

[9] A. Jehan, M. Husain, V. Tirth, A. Algahtani, M. Uzair, N. Rahman, and S.N. Khan, "Investigation of the structural, electronic, mechanical, and optical properties of $NaXCl_3$(X=Be, Mg) using density functional theory," RSC Advances, **13**, 28395 (2023).https://doi.org/10.1039/d3ra04922a

[10] A. Jehan, M. Husain, N. Sfina, S.N. Khan, N. Rahman, V. Tirth, R. Khan, *et al*., "First principles calculations to investigate structural, elastic, electronic, and optical properties of $XSrCl_3$(X=Li, Na)," Optik, **287**, 171088 (2023). https://doi.org/10.1016/j.ijleo.2023.171088

[11] A. Aqili, A.Y. Al-Reyahi, S.M. Al-Azar, S.S. Essaoud, M.E. Ketfi, M.E. Maghrabi, N. Al-Aqtash, and A. Mufleh, "Investigation the physical characteristics of inorganic cubic perovskite $CsZnX_3$(X=F, Cl, Br, and I): An extensive ab-initio study towards devices," Computational and Theoretical Chemistry, **1238**, 114721 (2024). https://doi.org/10.1016/j.comptc.2024.114721

[12] S. Ullah, M. Alshahrani, D. Alshehri, S. Tirth, V. Algahtani, A. Almalki, N. Rahman, *et al*., "First-principles insights into the structural, elastic, electronic, and optical properties of KHgX3 (X= F, Cl) novel halide perovskites," Indian Journal of Physics, 1-15 (2025). https://doi.org/10.1007/s12648-025-03878-5

[13] M. Arif, A. Reshak, S. Zaman, M. Hussain, N. Rahman, S. Ahmad, M. Saqib, *et al*., "Density functional theory based study of the physical properties of cesium based cubic halide perovskites $CsHgX_3$ (X=F, Cl)," International Journal of Energy Research, **46**, 2467-2476 (2022). https://doi.org/10.1002/er.7321
[14] S. Kirklin, J.E. Saal, B. Meredig, A. Thompson, J.W. Doak, M. Aykol, S. Rühl, and C. Wolverton, "The open quantum materials database (OQMD): assessing the accuracy of DFT formation energies," Nbj Comput. Mater. **1**, 1 (2015). https://doi.org/10.1038/npjcompumats.2015.10
[15] J. Saal, S. Kirklin, M. Aykol, B. Meredig, and C. Wolverton, "Materials design and discovery with high-throughput density functional theory: the open quantum materials database (OQMD)," JOM, **65**, 1501-1509 (2013). https://doi.org/10.1007/s11837-013-0755-4
[16] P. Blaha, K. Schwarz, G.A.H. Medsen, D. Kvasnicka, and J. Luitz, *WIEN2K: An Augmented Plane Wave Local Orbitals Program for Calculating Crystal Properties*, (Techn University, Wien, 2001).
[17] P. Blaha, K. Schwarz, P. Sorantin, and S.B. Trickey, "Full- Potential Linearized Augmented Plane Wave Program for Crystalline Systems," Comput. Phys. Commun. **59**, 399 (1990). https://doi.org/10.1016/0010-4655(90)90187-6
[18] W. Kohn, and L.J. Sham, "Self-consist equations including exchange and correlation effects," Phys. Review, **140**, A1133 (1965). https://doi.org/10.1103/physrev.140.a1133
[19] P. Hohenberg, and W. Kohn, "Density functional theory (DFT)," Phys. Review B, **136**, 864 (1964). http://dx.doi.org/10.1103/PhysRev.136.B864
[20] J.P. Perdew, S. Burke, and M. Ernzerhof, "Generalized gradient approximation made simple," Phys. Review. Lett. **77**, 3865 (1996). https://doi.org/10.1103/physrevlett.77.3865
[21] Z. Wu, and R.E. Cohen, "More accurate generalized gradient approximation for solids," Phys. Review B, **73**, 235116 (2006). https://doi.org/10.1103/physrevb.73.235116
[22] J.P. Perdew, A. Ruzsinszky, G.I. Csonka, O.A. Vydrov, G.E. Scuseria, L.A. Constantin, X. Zhou, *et al*., "Restoring the density-gradient expansion for exchange in solids and surfaces," Phys. Review Lett. **100**, 136406 (2008). https://doi.org/10.1103/physrevlett.102.039902
[23] F.D. Murnaghan, "The Compressibility of Media Under Extreme Pressure," Proc. Natl. Acad. Sci. USA, **30**, 244 (1944). https://doi.org/10.1073/pnas.30.9.244
[24] F. Tran, and P. Blaha, "Accurate band gaps of semiconductors and insulators with a semilocal exchange-correlation potential," Phys. Review. Lett. **102**, 226401 (2009). https://doi.org/10.1103/physrevlett.102.226401
[25] M. Jamal, S.J. Asadabadi, I. Ahmed, and H.R. Aliabad, "Elastic constants of cubic crystals," Comput. Mater. Sci. **95**, 592 (2014). https://doi.org/10.1016/j.commatsci.2014.08.027
[26] R. Ali, G.J. Hou, Z.G. Zhu, Q.B. Yan, Q.R. Zheng, and G. Su, "Stable mixed group II (Ca, Sr) and XIV(Ge, Sn) Lead-free perovskite solar cells," J. Mater. Chem. **6**, 9220 (2018). https://doi.org/10.1039/c8ta01490f
[27] Y. Zhou, and Y. Zhao, "Chemical stability and instability of inorganic halide perovskites," Energy & Environmental Science, **12**, 1495 (2019). https://doi.org/10.1039/c8ee03559h
[28] Y. Nassah, A. Benmakhlouf, L. Hadjeris, T. Helaimia, R. Khenata, A. Bouuhemadon, S. Bin-omran, *et al*., "Electronic, band structure, mechanical and optical characteristics of new lead-free halide perovskites for solar cell applications based on DFT computation," Bull. Mater. Sci. **46**, 55 (2023). https://doi.org/10.1007/s12034-023-02890-x
[29] F. Mouhat, and F.X. Coudert, "Necessary and sufficient elastic stability conditions in various crystal systems," Phys. Review, **90**, 224104 (2014). https://doi.org/10.1103/physrevb.90.224104
[30] J. Wang, S. Yip, S.R. Phillpot, and D. Wolf, "Crystal instabilities et finit strain," Phys. Review Lett. **71**, 4182 (1993). https://doi.org/10.1103/physrevlett.71.4182
[31] A.A. Mousa, M.S. Abu-Jafar, D. Dahbiah, R.M. Shaltaf, and J.M. Khalifeh, "Investigation of the perovskite $KSrX_3$(X=Cl and F) Compounds, Examining the optical, Elastic, Electronic, and Structural Properties: FP-LAPW Study," J. Electron. Mater. **47**, 641 (2018). https://doi.org/10.1007/s11664-017-5817-x
[32] W. Voight, *Lehrbuch des Kristallphysik*, (Teubnes, Leipzig, 1928).
[33] A. Reuss, "Berechnung der Fließgrenze von Mischkristallen auf Grund der Plastizitätsbedingung für Einkristalle," Z. angew. Math. Mech. **9**, 49 (1929). https://doi.org/10.1002/zamm.19290090104
[34] H. Fu, D. Li, F. Peng, T. Cao, and X. Cheng. "Ab initio calculations of elastic constants and thermodynamicproperties of NiAl under high pressures," Comput. Mater. Sci. **44**, 774 (2008). https://doi.org/10.1016/j.commatsci.2008.05.026
[35] G. Murtaza, R. Khenata, S. Mohamed, S. Naeem, M.N. Khalid, and A. Manzar, "Structural, elastic, electronic, and optical properties of $CsMCl_3$(M=Zn, Cd)," Physica B: Condensed Matter. **420**, 15 (2013). https://doi.org/10.1016/j.physb.2013.03.011
[36] I.N. Frantsevich, F.F. Voronov, and S.A. Bokuta, *Elastic Constants and Elastic Moduli of Metals and Insulators*, *Handbook*, (Naukuva Dumka, Kiev, 1983). pp. 60. (in Ukrainian)
[37] S.F. Pugh, "XCII. Relations between the elastic moduli and plastic properties of polycrystalline pure metals," (London, Edinburgh Dublin Philos. Mag. J. Sci. **45**, 823 (1954). https://doi.org/10.1080/14786440808520496
[38] D.G. Pettifor, "Theoretical predictions of structure and related properties of intermetallics," Mater. Sci. Techno. **8**, 345 (1992). https://doi.org/10.1179/mst.1992.8.4.345
[39] R. Gaillac, P. Pullumbi, F.-X. Coudert, "ELATE: an open-source online application for analysis and visualization of elastic tensors," J. Phys. Condens Matter, **28**, 275201 (2016). https://doi.org/10.1088/0953-8984/28/27/275201
[40] S.C. Wu, G.H. Fecher, S.S. Naghavi, and C. Felser, "Elastic properties and stability of Hensler compounds: Cubic Co_2YZ compounds with L_21 structure," J. Appl. Phys. **125**, 082523 (2019).https://doi.org/10.1063/1.5054398
[41] E. Schreibes, O.L. Anderson, and N. Soga, *Elastic Constants and Their Measurements*, (McGraw-Hill, NewYork,1996).
[42] L.O. Anderson, "A simplified method for calculating the Debye temperature from elastic constants," J. Phys. Chem. Solids, **24**, 909 (1963). https://doi.org/10.1016/0022-3697(63)90067-2
[43] M.E. Fine, L.D. Brown, and H.L. Marcus, "Electronic constants versus melting temperature in metals," Scr. Metall. **18**, 951 (1984). https://doi.org/10.1016/0036-9748(84)90267-9
[44] D.R. Penn, "Wave- number-dependent dielectric function of semiconductors," Phys. Review, **128**, 2093 (1960). https://doi.org/10.1103/physrev.128.2093

[45] M. Houari, B. Bouadjemi, S. Haid, M. Matoughui, T. Lantn, Z. Aziz, S. Bentata, and B. Bouhafs, "Semiconductors behavior of halide perovskites $AGeX_3$(A=K, Rb and Cs; X=F, Cl, and Br): First-principles calculations," Indian J Phys. **94**, 455 (2020). https://doi.org/10.1007/s12648-019-01480-0

[46] R. Sharma, A. Dey, S.A. Dar, and V. Srivastava, "A DFT investigation of $CsMgX_3$(X=Cl, Br) halide perovskites: Electronic, thermoelectric and optical properties," Computational and Theoretical Chemistry, **1204**, 113415 (2021). https://doi.org/10.1016/j.comptc.2021.113415

СТРУКТУРНІ, ОПТОЕЛЕКТРОННІ ТА МЕХАНІЧНІ ВЛАСТИВОСТІ ПЕРОВСКИТІВ AHgCl3 (A=Rb, Cs): АНАЛІЗ З ПЕРШИХ ПРИНЦИПІВ GGA ТА TB-mBJ

Хабіба Бухерауа, Ель-Джемаї Белбача

Лабораторія фізико-хімічних досліджень матеріалів (LEPCM), кафедра фізики, факультет наук про речовину, Університет Батна 1, 05000 Батна, Алжир

Структурні, механічні та оптоелектронні властивості кубічних галогенідних перовскітів $AHgCl_3$ (A = Rb, Cs) досліджували за допомогою теорії функціоналу густини (DFT) у рамках методу повнопотенціальної лінеаризованої доповненої плоскої хвилі (FP-LAPW), реалізованого в коді WIEN2k. Структурну стабільність кубічної фази підтверджували за допомогою коефіцієнта толерантності Гольдшмідта та октаедричного коефіцієнта, тоді як негативні енергії утворення підтвердили їх термодинамічну стабільність. Розраховані параметри пружності, включаючи коефіцієнт Пуассона, коефіцієнт П'ю та тиск Коші, вказують на те, що обидві сполуки є механічно стабільними, пластичними та переважно демонструють іонну природу зв'язків. Оптоелектронні властивості досліджували за допомогою модифікованого потенціалу Бекке-Джонсона Трана-Блаха (TB-mBJ). Результати показують, що $RbHgCl_3$ та $CsHgCl_3$ є напівпровідниками з непрямою забороненою зоною та шириною забороненої зони 1,25 еВ і 1,16 еВ відповідно. Крім того, оптичні властивості були проаналізовані в діапазоні енергії фотонів 0–20 еВ. Обидві сполуки демонструють сильне поглинання в ультрафіолетовому діапазоні та низьку відбивну здатність за нульової енергії фотонів, що вказує на сприятливі характеристики для оптоелектронних застосувань. Загалом, ці результати свідчать про те, що галогенідні перовскіти $AHgCl_3$ (A = Rb, Cs) є перспективними кандидатами для застосування у фотоелектричних пристроях та ультрафіолетових фотодетекторах.

Ключові слова: *галогенідні перовскіти $KZnX_3$; FP-LAPW; ab-initio; Wien2k; оптоелектронні властивості; TB-mBJ*